J. Fluid Mech. (1988), *vol.* 186, *pp.* 243–256
Printed in Great Britain

An experimental investigation of the flow of non-Newtonian fluids between rotating disks

By A. SIRIVAT, K. R. RAJAGOPAL AND A. Z. SZERI
Department of Mechanical Engineering, University of Pittsburgh, Pittsburgh, PA 15261, USA

(Received 8 December 1986 and in revised form 17 May 1987)

The results of an experimental investigation on the flow of a non-Newtonian fluid between rotating, parallel disks are described in this paper. These results are qualitatively different from those exhibited by linearly viscous fluids in that a narrow layer of exceedingly high velocity gradients appears in the non-Newtonian fluid.

1. Introduction

Few problems in fluid mechanics have enjoyed the attention that has been accorded to the flow that occurs due to the rotation of a single disk or that between two rotating disks. Kármán (1921) introduced an ingenious similarity transformation which reduced the Navier–Stokes equations into a set of coupled nonlinear ordinary differential equations. This pioneering study has been followed by an innumerable number of papers which span the whole gamut from experimental papers to those which concern themselves with mathematical queries regarding existence and uniqueness. An up-to-date review of the relevant literature can be found in the articles by Parter (1982) and Rajagopal (1987).

In this paper, we shall present the results of an experimental investigation on the flow of a non-Newtonian fluid (Polyacrylamide solution) between two disks rotating with differing angular speeds about a common axis. The experimental results are qualitatively different from those exhibited by linearly viscous fluids. The results very clearly suggest the appropriate class of non-Newtonian-fluid models from amongst the many that are available. We shall discuss this in detail later. Previous work that is of relevance to our investigation begins with Batchelor (1951) who showed that the similarity transformation introduced by Kármán would also be appropriate for studying the flow of a linearly viscous fluid between two infinite parallel disks rotating with constant but differing angular speeds about a common axis. Batchelor (1951) predicted that at high Reynolds numbers boundary layers would develop on each disk and the core of the fluid would rotate at a constant angular speed. Later, Stewartson (1953) in analysing the same problem came to a totally different conclusion. He argued that the flow in the core region would be purely axial. Since then, there have been several studies aimed at resolving this question (cf. Lance & Rogers 1961; Pearson 1965; Mellor, Chapple & Stokes 1968; Greenspan 1972; Schultz & Greenspan 1974; Roberts & Shipman 1976; Nguyen, Ribault & Florent (1975); Pesch & Rentrop 1965; Wilson & Schryer 1978; Holodniok, Kubicek & Hlavacek 1978, 1981; Adams & Szeri 1982; Dijkstra & van Heijst 1983). The numerical studies indicate that both the Batchelor type and the Stewartson type of solutions are possible. The numerical studies of Dijkstra & van Heijst (1983), Adams & Szeri (1982) and Szeri *et al.* (1983) were on flows between

finite disks. For the case of flow between infinite rotating disks the numerical studies clearly show that the Navier–Stokes equations possess multiple solutions, in fact possibly an infinity of them.

The similarity transformation of Kármán assumes that the flow under consideration is rotationally symmetric. Recently, Berker (1979) showed that when the two disks are rotating with the same angular speed, there exists a one-parameter family of solutions all but one of which are not rotationally symmetric. This result has been extended by Parter & Rajagopal (1984), for the disks rotating with differing angular speeds, who prove that the rotationally symmetric solutions are never isolated when considered within the full scope of the Navier–Stokes equations. A detailed numerical study of the asymmetric flow has been carried out by Lai, Rajagopal & Szeri (1984).

Recently, there has been a considerable amount of interest in the flow of non-Newtonian fluids between rotating disks, since the flow geometry is one which has several technical applications, for example lubrication. Unlike the earlier studies on linearly viscous fluids, studies on non-Newtonian fluids are rendered more complicated by our having first to decide on a proper choice for the constitutive equation for the fluid under consideration. Depending on the model that is employed, we might obtain totally different governing equations for the problem under consideration. Much of the analytical work that has been carried out thus far is restricted to fluid models of the differential type (cf. Truesdell & Noll 1965). We shall not discuss in detail the many specific fluid models of the differential and the rate type which have been employed, as we shall see that none of these models can adequately describe the experimental results that have been established. The recent work of Huilgol & Keller (1985) on the flow of an Oldroyd fluid (cf. Oldroyd 1950) includes many of the previous studies as special examples. Recently, Huilgol & Rajagopal (1987) have shown that, similar to the linearly viscous case, solutions that are not axially symmetric are possible in the case of an Oldroyd fluid. We refer the reader to Rajagopal (1987) for a discussion of some of the work that has been carried out in the area.

A marked departure in the flow characteristics of the non-Newtonian fluid under consideration from that of a Newtonian fluid is the existence of a narrow layer wherein the velocity gradients are exceedingly high. It is felt that this narrow layer is a result of 'shear thinning' which takes place in certain non-Newtonian fluids. This phenomenon cannot be explained in terms of the popular fluids of the differential type, e.g. an incompressible homogeneous fluid of second grade (cf. Truesdell & Noll 1965), or the Oldroyd fluid (cf. Oldroyd 1950). Of course, 'shear thinning' could be described if the material moduli which characterize those models are not assumed constant but as functions of the principal invariants of the stretching. However, in the absence of a rational means for choosing these material functions, we feel it would be appropriate to use integral models which have been used successfully in describing 'shear thinning'. Amongst the many integral models that have been used to describe non-Newtonian fluid behaviour, the K–BKZ fluid model (cf. Kaye 1962; Bernstein, Kearsely & Zapas 1963) has been accepted by both the theoretician and the experimentalist. This model has also been shown to be consistent with the statistical approach used in modelling polymeric fluids. The class of K–BKZ models includes a variety of models like the Wagner one (cf. Wagner 1976) which is particularly appropriate in describing shear thinning in non-Newtonian fluids. We feel that the Wagner model is generally enough to model the shear layer that we observe, while

at the same time it is not too complicated to make a theoretical analysis impossible.

The earliest experiment on the flow between two rotating disks was carried out by Stewartson (1953). He studied the flow of air due to the rotation of two cardboard disks to obtain some qualitative information regarding the flow. Other experiments have been carried out by Gregory, Stuart & Walker (1955) and Faller (1963). These earlier works used either a hot wire or flow-visualization techniques. Recently, Szeri *et al.* (1983) have carried out a detailed experimental investigation of the flow between finite rotating disks using a laser-Doppler velocimeter. Their measurements show the existence of a velocity field as conjectured by Batchelor (1951).

With regard to non-Newtonian fluids, there are few experiments on flow between disks rotating with distinct angular speeds about a common axis. Connelly & Greener (1985) have made gross measurements of the forces and torques in order to determine the rheological properties of non-Newtonian fluids at high shear rates. However, there are no experiments in which finer local measurements, like the velocity field, have been carried out. This aspect of the experimentation is the primary object of our study. The velocity field is measured by means of a laser-Doppler velocimeter. A detailed description of the set-up is provided later (cf. figure 1).

Our experiments were carried out on 0.029% and 0.053% by weight solutions of Polyacrylamide. Tangential and radial velocities were measured for a variety of rotation rates. At low rotation rates, the tangential velocity profile varies nearly linearly with z. But as the rotation rate is increased, boundary layers develop. However, these velocity profiles are drastically different from those observed in water. This marked contrast is due to the existence of an exceedingly thin 'shear layer' close to the rotating disk and none appears near the stationary plate. We find that the effect becomes even more pronounced at higher rotation rates. As the concentration of the Polyacrylamide solution is changed from 0.029% to 0.053%, the flow field is qualitatively similar in that a shear layer once again manifests itself, with minor quantitative differences. Thus, the major qualitative change occurs as one substitutes a non-Newtonian Polyacrylamide solution, even when it is diluted, for the Newtonian water, and not when the concentration of the non-Newtonian fluid is varied.

2. Experimental set-up

2.1. *The rotating disk apparatus*

The apparatus is the same as that used in the experiments of Szeri *et al.* (1983). It consists of two 50.8 cm diameter disks, the upper one of Plexiglas and the lower of polished aluminium as shown in figure 1. The top disk is part of the entire enclosure and the wall. Both disks are connected to two concentric shafts which are supported by two sets of bearings and drawn by two independent constant-torque a.c. motors by means of V-belts and pulleys. The disk separation h is fixed at 1.27 cm, giving the aspect ratio, defined as the ratio of the radius to the gap, as 20, where R_0 is the disk radius.

The fluid can be gravity fed into the appratus from the centre of the bottom disk through a hole of radius 1.69 cm which is connected to a feed tube in the centre of the inner shaft, and can be drained through an annular tube located within the inner shaft. The fluid circulation system consists of a lower reservoir, a pump and an upper reservoir which has a maximum capacity of 40 gallons. The main purpose of the

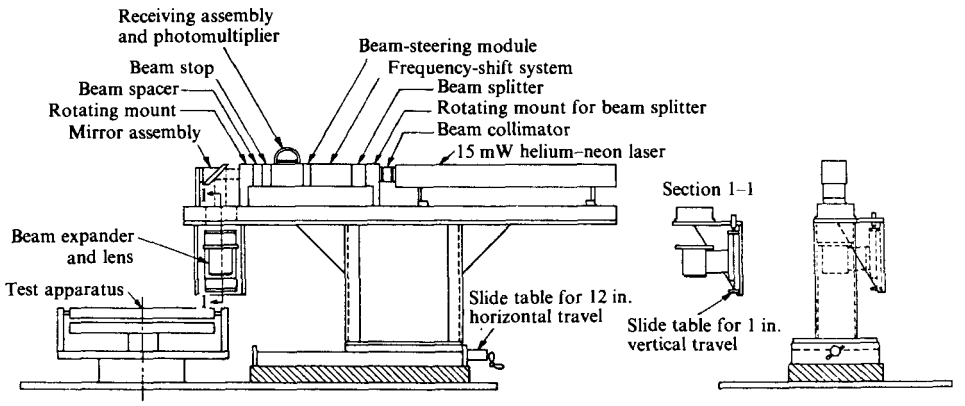

FIGURE 1. Experimental set-up: the rotating-disk apparatus and the laser-Doppler velocimeter.

circulation system in this experiment is to bleed off bubbles, which form at the upper Plexiglas disk, by means of three bleed valves located at the top of the enclosure. Two slide tables allow the positioning of the probe volume within the flow in both the radial and axial directions.

The dilute polymer solution used is a mixture of Polyacrylamide (Dow Chemical, Sepparan MG-700) and deionized water with concentration of 290 p.p.m. and 530 p.p.m. by weight. The deionized distilled water was first mixed with a small amount of sodium silicate and sodium nitrate to provide additional corrosion protection. The parts of the apparatus that are in contact with the solution are the upper reservoir (stainless steel), the lower reservoir (aluminium), the disks and the enclosure (chrome plating and aluminium) and plastic pipes. A small volume of Biosite was added to keep the water clean and clear from possible bacteria contamination. The total mixture of 15 gallons was first prepared in separate tanks by adding Polyacrylamide in small amounts and gently stirring. Initially some gels were found owing to inadequate mixing and the solution was left in the tank for 48 h with periodic stirring until all visible gels vanished. The solution was then transferred to the apparatus. Nearly all the bubbles were then removed through the bleeding valves; some small bubbles were left outside the disk area but these would not affect the velocity field in any way.

The selection of the Polyacrylamide was based on several factors. Because of its high molecular weight, $8\text{–}10 \times 10^6$, its solutions are known to exhibit highly elastic and strongly shear-thinning behaviour (Bruce & Schwartz 1969; Connelly & Greener 1985). Secondly, it is relatively stable to shear, despite many other possible sources of degradation which will be later discussed. It also forms a clear solution, and is nearly odourless and generally non-toxic. In addition, its rheological properties are well documented.

2.2. *The laser-Doppler velocimetry*

The velocity field is measured by a laser-Doppler velocimeter, operated in the back-scatter/dual-beam mode. The system consists of a 15 mW helium–neon laser (Spectral Physics, model 9124), a beam collimator, a beam splitter, a Bragg cell which shifts one frequency of the beam, a beam steering module, a beam stopper, a 45° mirror, a beam expander and a focusing lens; all of the above optical components are from TSI. Figure 1 shows details of the optical set-up. The measuring volume

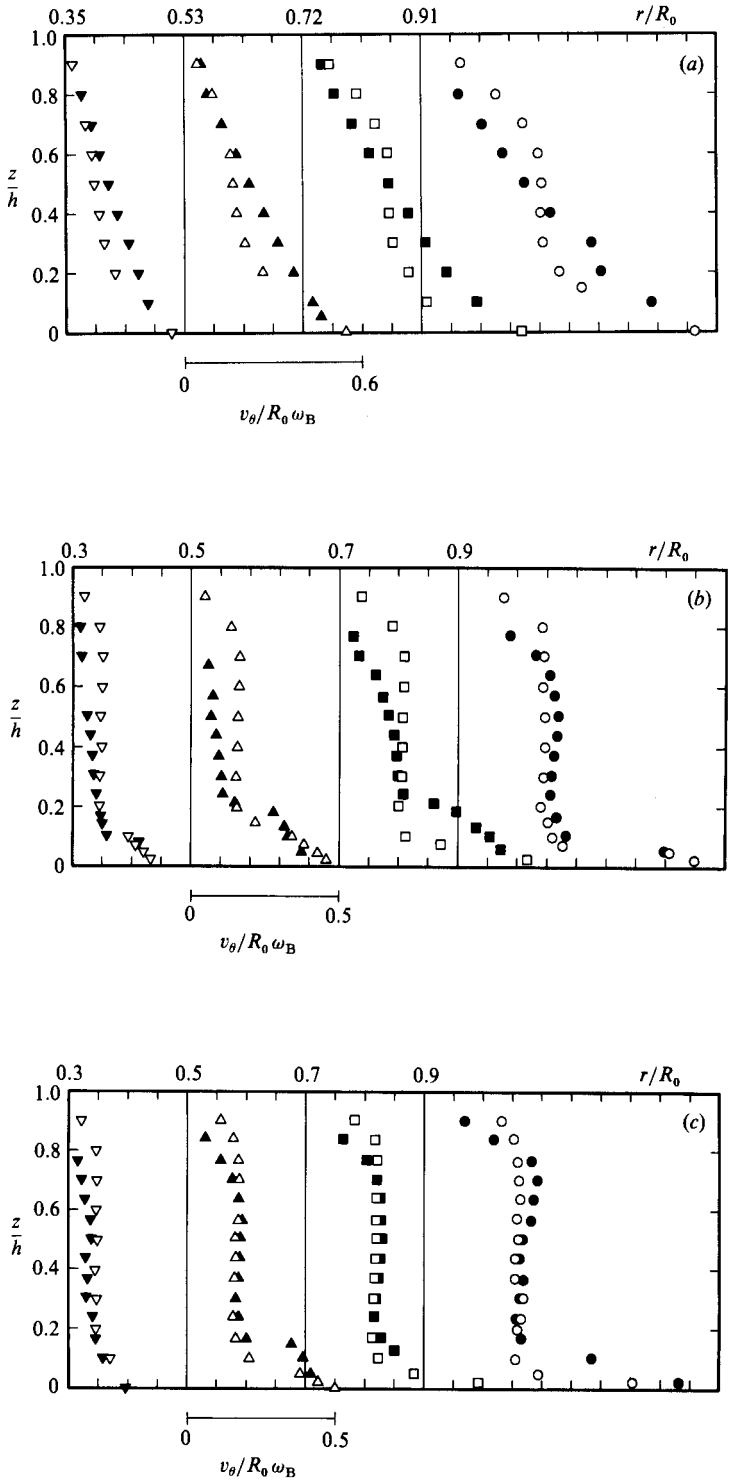

FIGURE 2. Tangential velocity profiles of the polymer solution ($C = 0.029\%$) and of the solvent water. The solid symbols are for the polymer solution and the open symbols are for the solvent water; (*a*) $\omega_B = 0.285$ rad/s ($N_B = 2.72$ r.p.m.); (*b*) 2.20 rad/s (21.0 r.p.m.); (*c*) 4.712 rad/s (45 r.p.m.).

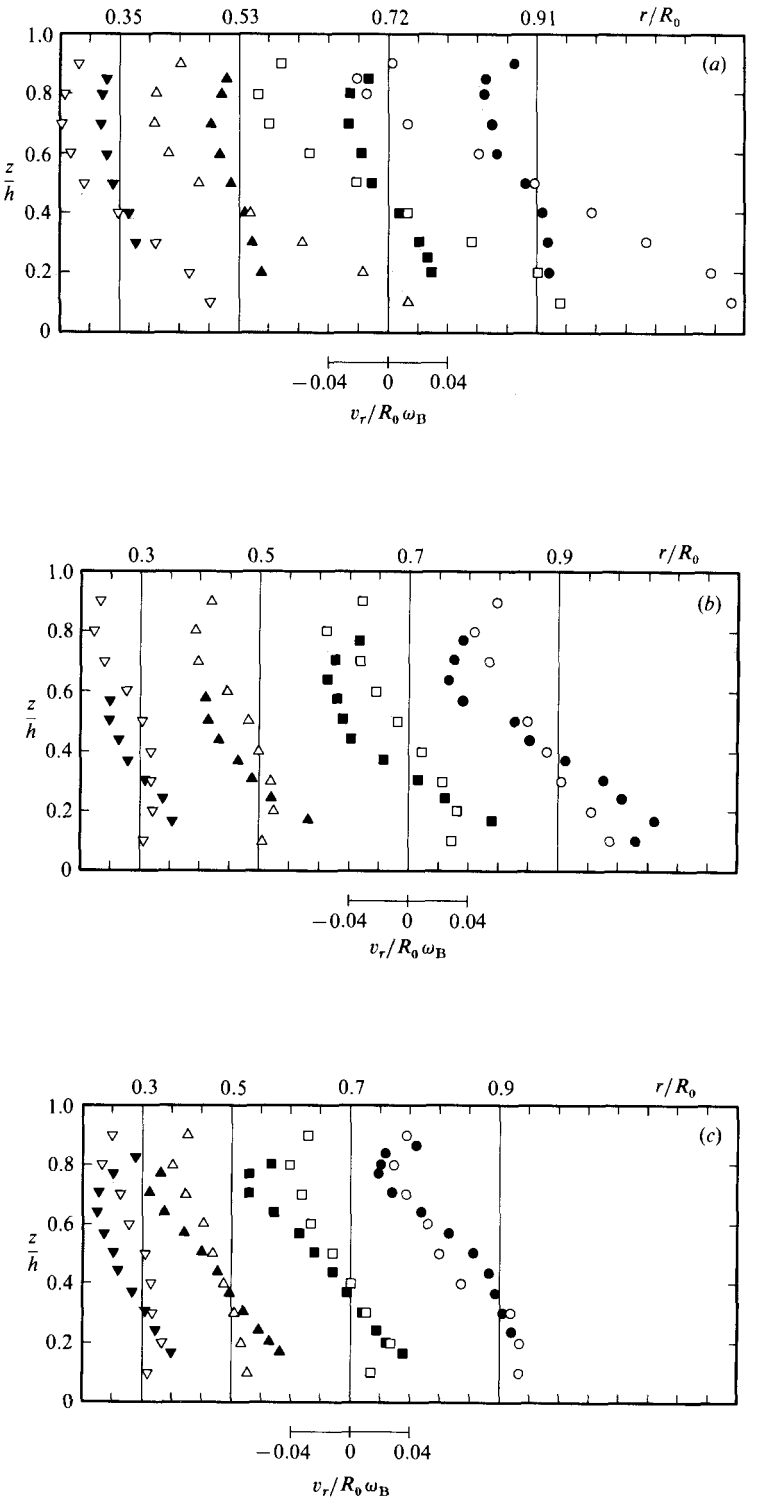

FIGURE 3. Radial velocity profiles of the polymer solution ($C = 0.029\%$) and of the solvent water. The solid symbols are for the polymer solution and the open symbols are for the solvent water: (*a*) $\omega_B = 0.285$ rad/s ($N_B = 2.72$ r.p.m.); (*b*) 2.20 rad/s (21.0 r.p.m.); (*c*) 4.712 rad/s (45 r.p.m.).

length l_m and the probe volume diameter d_m are calculated to be 0.193 mm and 0.0365 mm respectively, based on the wavelength λ of 632.8 nm, collimated beam diameter of 1.2 mm, the lens focal length f of 121.4 mm and half the beam intersection angle of 10.725°. The fringe spacing is then 1.7002 μm and the number of fringes within the volume is 20. The ratio of the disk spacing h and the probe diameter in our experiment is above 600, allowing one to measure the velocity profiles in detail. Thus the spatial resolution of the measured velocity field is limited by the mechanically traversing table which is accurate only to 0.25 mm. The particles used to seed the flow are of silicon carbide with a mean diameter of 1.5 μm, refractive index of 2.65 and density of 3.2 g/cm^3.

The scattered light from the measuring volume is picked up by a photomultiplier tube through the same optical components as used in transmitting the beams. The signal is passed through a variable band-pass filter (Ithaco) before being analysed by a counter (TSI 1980). The output of a counter in analog form is analysed by a digital oscilloscope for the mean and standard-deviation calculations.

3. Experimental results

The velocity fields

Figure 2(*a–c*) shows the tangential velocity profiles normalized by $R_0\omega_B$, where R_0 is the disk outer radius and $\omega_B = 0.283$ rad/s (2.7 r.p.m.). At lower disk angular speeds the velocity profiles of the polymer solution ($C = 0.029\%$) are nearly linear with respect to the axial coordinate z. On the other hand, the velocity profiles for the pure solvent (water) show progressive development of a Batchelor-type profile (Batchelor 1953) along the radial direction; the main core of the fluid rotates at a uniform angular velocity relative to the disk with the formation of two boundary layers, one on the stationary disk (Bödewadt) and one on the rotating disk (Kármán 1921). At a higher disk angular speed, $\omega_B = 2.19$ rad/s ($N_B = 21$ r.p.m.), the velocity profiles for the polymer solution resemble those of the pure solvent at the lower ω_B of 0.283 rad/s. However, a qualitative difference appears to be the flow field adjacent to the rotating disk due to a formation of a new boundary layer. At the highest angular speed of $\omega_B = 4.71$ rad/s ($N_B = 45$ r.p.m.), the velocity profile for the polymer solution and that for the solvent are such that in their respective main cores they rotate at a nearly identical angular velocity. A slight difference is noticeable in the profile of $r/R_0 = 0.9$ where the angular momentum of the polymer solution is slightly higher than that for the solvent. Generally, the boundary layer at the stationary disk is thicker for the polymer solution.

Figure 3(*a–c*) shows the corresponding radial velocity profiles (normalized by $R_0\omega_B$ for both the solvent and the polymer). Any fluid particle near the rotating disk is thrown outward due to the centrifugal effect causing a radial outflow near the rotating disk. This same fluid particle is then returned near the stationary disk thus forming a single cell in the meridian plane (r, z) for both the solvent and the polymer solution. The observed difference is that the polymer fluid particles decelerate earlier above the rotating disk at large r/R_0 owing to the presence of the stationary cylindrical wall. The magnitudes of the secondary flow are smaller everywhere for the polymer solution than for the solvent at the low disk angular speed. However, as the disk speed is increased, two qualitative differences are observed. First, the cell of the polymer fluid is tilted resulting in departure from symmetric radial velocity profiles. Secondly, the normalized magnitudes of the secondary flow increase and exceed those of the Newtonian fluid.

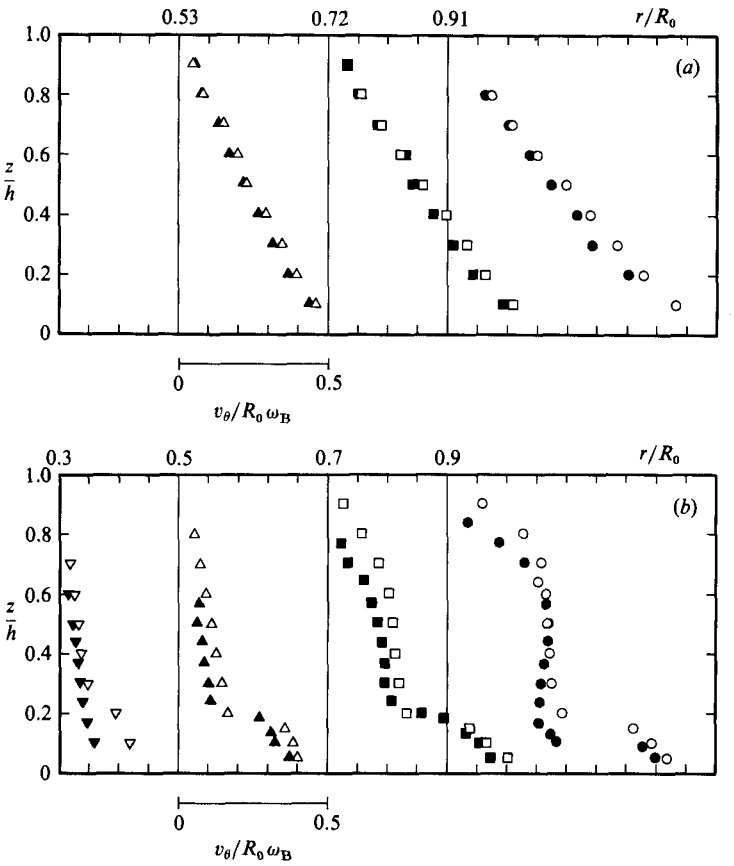

FIGURE 4. Comparisons of the tangential velocity profiles for two concentrations of the polymer solution. The solid symbols are for $C = 0.029\%$, the open symbols for $C = 0.053\%$: (*a*) $\omega_B = 0.285$ rad/s ($N_B = 2.72$ r.p.m.); (*b*) 2.20 rad/s (21.0 r.p.m.).

Figures 4 and 5 compare the velocity profiles for the polymer solutions at two concentraions of $C = 0.029\%$ and 0.053%. The tangential-velocity-component magnitudes increase with increasing concentration of the polymer solution at both the low $\omega_B = 0.283$ rad/s and the higher $\omega_B = 2.19$ rad/s.

Figure 6(*a–d*) shows a series of experimental data for $V_\theta/R_0\omega_B$ at $r/R_0 = 0.5$ and $C = 0.029\%$ as the angular speed of the bottom disk is increased from $\omega_B = 0.142$ rad/s ($N_B = 1.36$ r.p.m.) to $\omega_B = 4.712$ rad/s ($N_B = 45$ r.p.m.). At the lowest rotational speed, the velocity profile is trivial; it varies linearly with z, the axial coordinate. Initially, the effect of increasing the angular velocity of the bottom disk is to cause the velocity profile to deviate from linearity. At approximately $\omega_B = 0.85$ rad/s, it is possible to notice the formation of a yielding zone which coincides with the inflexion point, at $z/h \approx 0.15$. With further increase in the angular speed a 'shear layer' develops at a certain distance from the rotating wall, even though the no-slip condition at the wall still applies. The shear layers are shown in the figure 6(*b*).

In figure 6(*c*), the effect of increasing ω_B from 2.2 to 3.08 rad/s appears to be the expansion of the main core of the nearly rigid-body rotation as well as changing the shear layer gradient and its location. Figure 6(*d*) shows the boundary layers for angular speeds from $\omega_B = 3.5$ to 4.7 rad/s. In this range of the bottom-disk speed, the

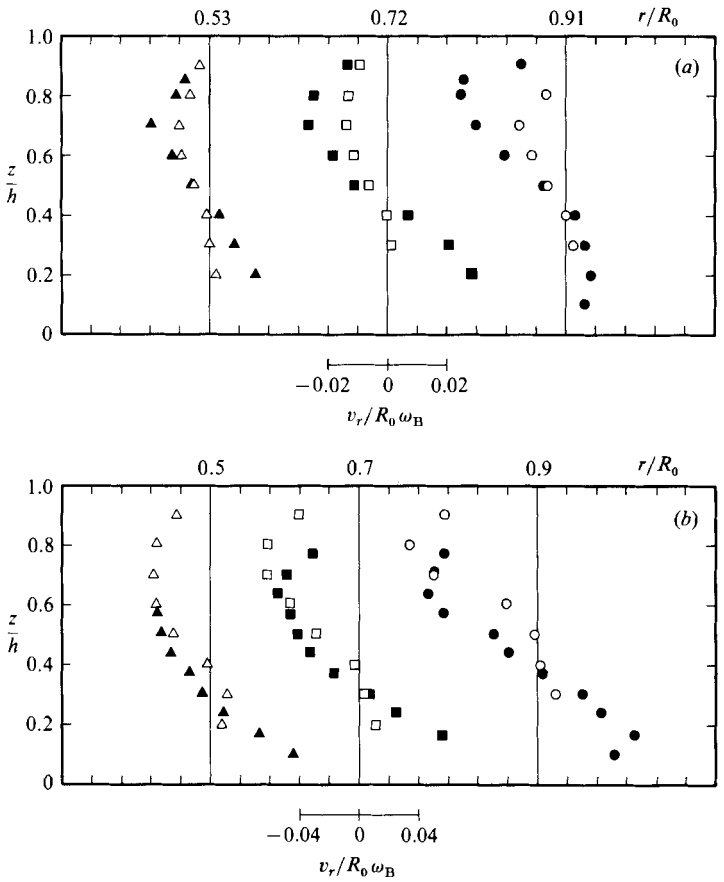

FIGURE 5. Comparisons of the radial velocity profiles for two concentrations of the polymer solution. The solid symbols are for $C = 0.029\,\%$, the open symbols for $C = 0.053\,\%$: (*a*) $\omega_B = 0.285$ rad/s ($N_B = 2.72$ r.p.m.); (*b*) 2.20 rad/s (21.0 r.p.m.).

normalized velocity is nearly independent of ω_B for most of the flow with the exception of perhaps the region close to the wall.

Figure 7 (*a*, *b*) shows the effect of concentration on the boundary layer and the shear layer. For a given angular velocity ω_B, the boundary layers are identical and independent of C for the region close to the wall, whereas both the slip layer and the formation of the main core of the nearly solid-body rotation are affected by a change in concentration. Thus the overall effect of the concentration seems to be confined to a region away from the wall.

Figure 8 shows a plot of the tangential velocity component as would be observed in a frame rotated at the disk angular velocity ω_B ,normalized with wall friction velocity $(\omega_B/\nu)^{\frac{1}{2}}$. The boundary layer here shows that the viscous sublayer is confined to within about a viscous length unit of $(\nu/\omega_B)^{\frac{1}{2}}$, followed by the buffer layer spanning between $z^+ = z\ (\omega_B/\nu)^{\frac{1}{2}}$ of 1 and 4. The slip-layer thickness is also approximately equal to the viscous lengthscale. The slip velocity seems to be insensitive to the change in concentration in the range of concentration investigated. The effect of the increase in the polymer concentration only appears outside the shear layer, resulting in a slight flow enhancement relative to the rotating disk.

Figure 9 (*a*) shows the shear-layer position, at the non-dimensional distance δ/h

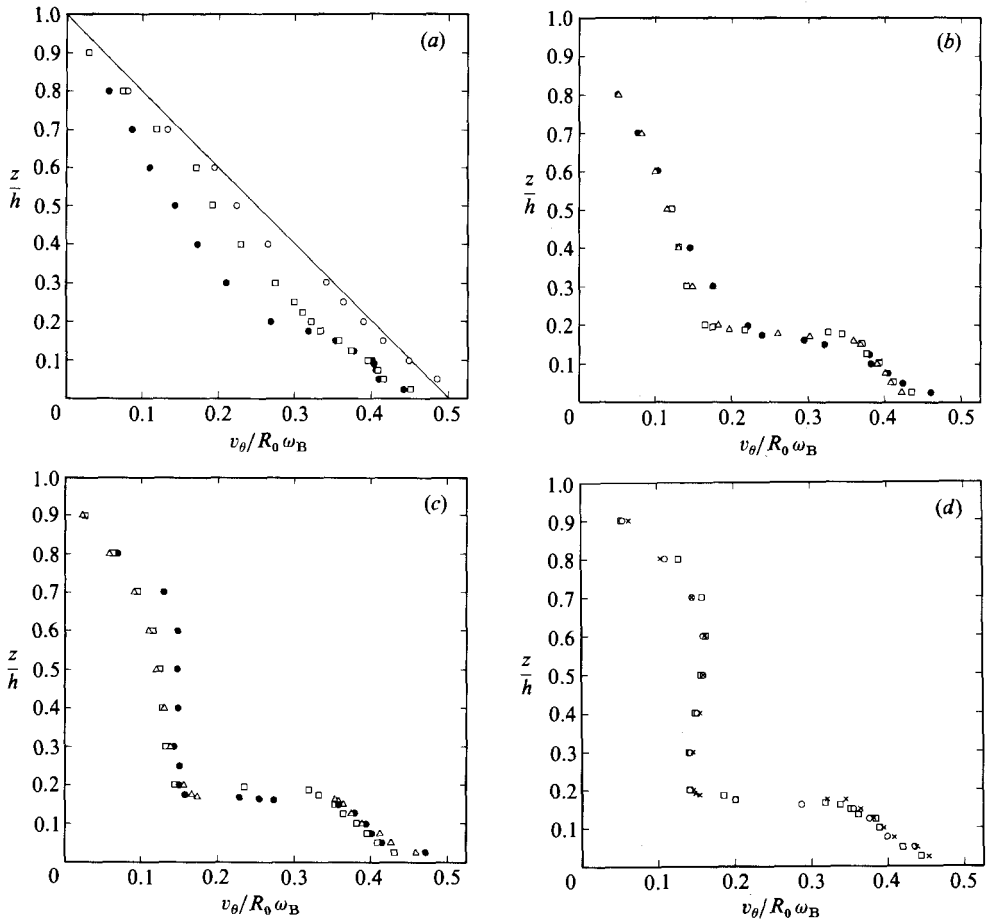

FIGURE 6. The boundary layers on a rotating disk at different rotation rates showing the formation of the slip layer. The measurements were taken at $r/R_0 = 0.5$. (*a*) ○, $\omega_B = 0.142$ rad/s ($N_B = 1.35$ r.p.m.); □, 0.424 rad/s (4.05 r.p.m.); ●, 0.848 rad/s (8.1 r.p.m.). (*b*) ●, 1.099 rad/s (10.5 r.p.m.); △, 1.59 rad/s (15.2 r.p.m.); □, 1.95 rad/s (18.6 r.p.m.). (*c*) △, 2.199 rad/s (21.0 r.p.m.); □, 2.544 rad/s (24.3 r.p.m.); ●, 3.08 rad/s (29.4 r.p.m.). (*d*) ×, 3.497 rad/s (33.4 r.p.m.); ○, 3.905 rad/s (37.3 r.p.m.); □, 4.712 rad/s (45.0 r.p.m.).

from the rotating disk, plotted in terms of the Ekman number $Ek^{-1} = h^2\omega_B/\nu$, where ν is the kinematic viscosity of the solvent water. The shear-layer position is defined here to be the distance from the rotating disk to the position where the velocity gradient is maximum. For a given r/R_0, δ/h increases with ω_B just after the onset of the shear layer and then appears to decrease indefinitely as ω_B increases. Thus the shear-layer position, which is observed to be away from the wall, will be closer to the rotating wall as ω_B increases further and eventually creates the so-called wall-slip condition even though the viscous sublayer still adheres to the wall. The effect of change in concentration is hardly noticeable with the exception that the onset of the shear layer occurs at a lower ω_B for the lower-concentration solution. The situation at $r/R_0 = 0.9$ is slightly different in that the shear-layer position increases again as ω_B is increased. This may be partly due to the rotating-disk edge effect where the axial flow in the z-direction becomes appreciable near the disk edge at large ω_B.

Figure 9 (*b*) shows the magnitude the slip V_s normalized with the local characteristic

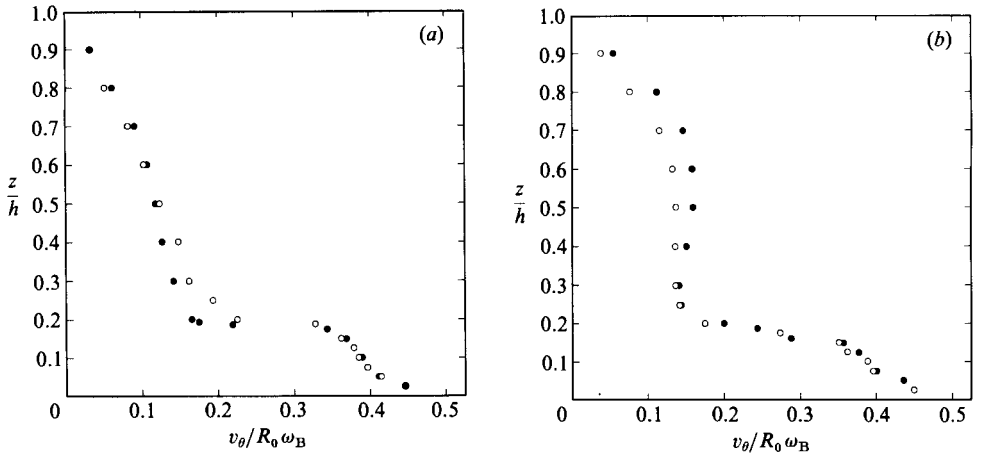

FIGURE 7. The effect of the polymer concentration on the boundary layer. The measurements were taken at $r/R_0 = 0.5$; ●, $C = 0.029\%$; ○, 0.053%. (*a*) $\omega_B = 1.947$ rad/s ($N_B = 18.6$ r.p.m.); (*b*) 3.905 rad/s (37.3 r.p.m.).

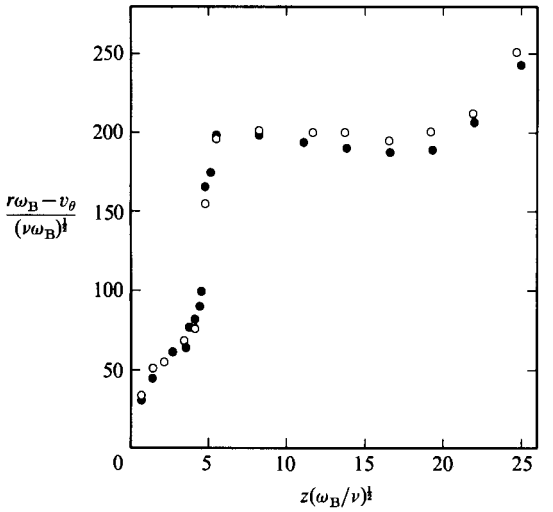

FIGURE 8. Normalized velocity profiles using $(\nu\omega_B)^{\frac{1}{2}}$ as the characteristic velocity scale, $\omega_B = 3.905$ rad/s ($N_B = 37.3$ r.p.m.). ●, $C = 0.029\%$; ○, 0.053%.

velocity $r\omega_B$ in terms of the Ekman number Ek. Here the slip velocity is defined to be the difference between the edges of the shear layer. The effect of concentration on the slip velocity is slight.

4. Discussion of the results

It is well known that a polymer solution will age or degrade when subjected to a strong shear rate, or its rheological properties may change as a result of chemical or bacterial effects. In the present flow, the shear rate is moderately high and some mechanical pumping was required occasionally in the flow set-up. Figure 10 shows the tangential velocity profiles at two ω_B values, taken on two occasions approximately 3 months apart. For the flow with $\omega_B = 0.64$ rad/s, the profiles were

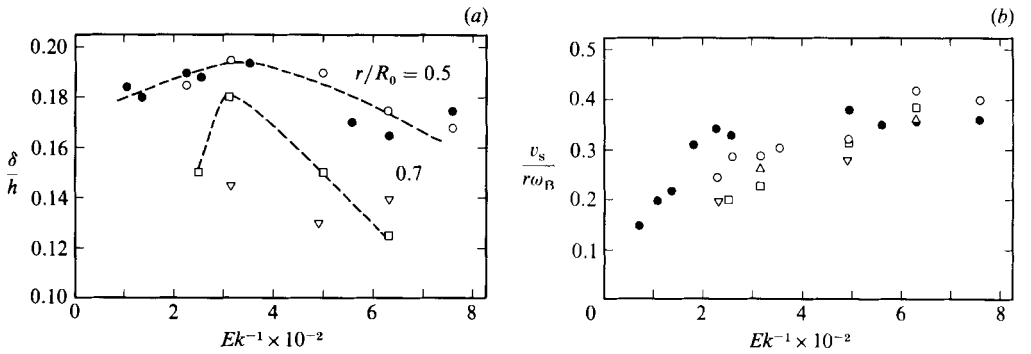

FIGURE 9. The slip-layer characteristics in terms of the Ekman number $Ek^{-1} = h^2\omega_B/\nu$: ●, $C = 0.029\%$, $r/R_0 = 0.5$; ○, 0.053%, 0.5; □, 0.05; □, 0.053%, 0.7; ▽, 0.053%, 0.9; △, 0.053%, 0.4. (*a*) The position of the shear layer from the rotating wall, δ/h. (*b*) The magnitude of the velocity difference in the shear layer, $\Delta v_s/r\omega_B$.

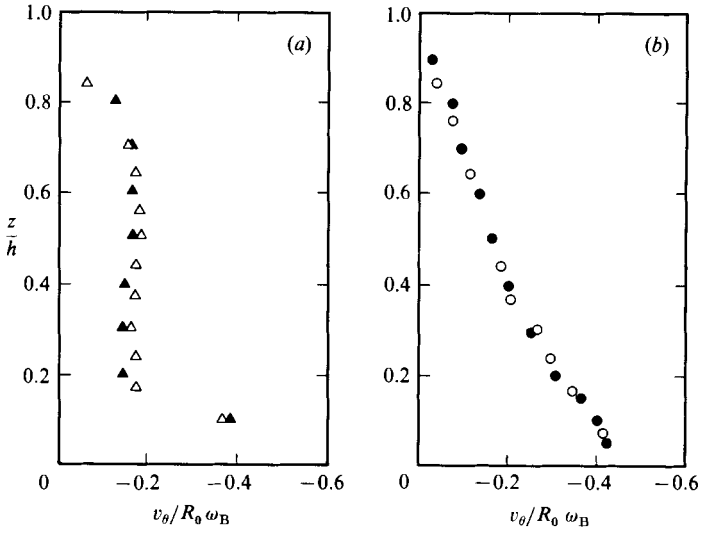

FIGURE 10. The degradation effects on the velocity profiles. The open symbols are for the older data and the solid symbols are for the most recent data. Concentration is 0.029%. (*a*) $\omega_B = 0.639$ rad/s; (*b*) 4.712 rad/s.

nearly reproducible within 2% whereas for the high $\omega_B = 4.712$ rad/s the profiles show relative differences of approximately 6% (cf. figure 10). Thus it appears that degradation which occurs on the molecular level does affect the flow field (the bulk velocity) only slightly, the degree of change depending upon the shear rate of the flow. It is also possible that the Polyacrylamide was already in the stable state during the experiment period. The chemical effect due to interaction of the solution with the wall was possibly minor in our experiment since none of the apparatus parts in contact with the solution is of brass or ferrous materials.

This material is based upon work partially supported by the National Science Foundation under Grants MEA-7821853 and MEA-8410724. This support is gratefully acknowledged.

REFERENCES

ADAMS, M. L. & SZERI, A. Z. 1982 Incompressible flow between finite disks. *Trans. ASME* E: *J. Appl. Mech.* **49**, 1–14.

BATCHELOR, G. K. 1951 Note on a class of solutions of the Navier–Stokes equations representing steady rotationally-symmetric flow. *Q. J. Mech. Appl. Maths* **4**, 29–41.

BERKER, R. 1979 A new solution of the Navier–Stokes equation for the motion of a fluid contained between two parallel planes rotating about the same axis. *Archiwum Mechaniki Stosowanej* **31**, 265–280.

BERNSTEIN, B., KEARSLEY, E. A. & ZAPAS, L. J. 1963 A study of stress relaxation with finite strain. *Trans. Soc. Rheol.* **7**, 391–410.

CONNELLY, R. W. & GREENER, J. 1985 High-shear viscometry with a rotational parallel-disk-device. *J. Rheol.* **29**, 209–226.

DIJKSTRA, D., & VAN HEIJST, G. J. F. 1983 The flow between finite rotating disks enclosed by a cylinder. *J. Fluid Mech.* **128**, 123–154.

FALLER, A. J. 1963 An experimental study of the instability of the laminar Ekman boundary layer. *J. Fluid Mech.* **15**, 560–576.

GREENSPAN, D. 1972 Numerical studies of flow between rotating co-axial disks. *J. Inst. Maths. Applics* **9**, 370–377.

GREGORY, N., STUART, J. T. & WALKER, W. S. 1955 On the stability of three dimensional boundary layers with application to the flow due to a rotating disk. *Phil. Trans. R. Soc. Lond.* A **248**, 155–199.

HOLODNIOK, M., KUBICEK, M. & HLAVACEK, V. 1978 Computation of flow between two rotating co-axial disks. *J. Fluid Mech.* **81**, 579–596.

HOLODNIOK, M., KUBICEK, M. & HLAVACEK, V. 1981 Computation of flow between two rotating co-axial disks: multiplicity of steady state solutions. *J. Fluid Mech.* **108**, 227–240.

HUILGOL, R. R. & KELLER, J. B. 1985 Flow of viscoelastic fluids between rotating disks: Part 1. *J. Non-Newtonian Fluid Mech.* **18**, 101–110.

HUILGOL, R. R. & RAJAGOPAL, K. R. 1987 Non-axisymmetric flow of a viscoelastic fluid between rotating disks. *J. Non-Newtonian Fluid Mech.* **23**, 423–434.

KÁRMÁN, T. VON 1921 Über laminare und turbulente Reibung. *Z. Angew. Math. Mech.* **1**, 232–252.

KAYE, A. 1962 *Note* 134. College of Aeronautics, Cranfield Institute of Technology.

LAI, C.-Y., RAJAGOPAL, K. R. & SZERI, A. Z. 1984 Asymmetric flow between parallel rotating disks. *J. Fluid Mech.* **146**, 203–225.

LANCE, G. N. & ROGERS, M. H. 1961 The axially symmetric flow of a viscous fluid between two infinite rotating disks. *Proc. R. Soc. Lond.* A **266**, 109–121.

MELLOR, G. L., CHAPPLE, P. J. & STOKES, V. . 1968 On the flow between a rotating and a stationary disk. *J. Fluid Mech.* **31**, 95–112.

NGUYEN, N. D., RIBAULT, J. P. & FLORENT, P. 1975 Multiple solutions for the flow between co-axial disks. *J. Fluid Mech.* **68**, 369–388.

OLDROYD, J. G. 1950 On the formation of rheological equations of state. *Proc. R. Soc. Lond.* A **200**, 523–541.

PARTER, S. V. 1982 On the swirling flow between rotating co-axial disks: A survey. In *Theory and Applications of Singular Perturbations, Proc. of a Conf. Oberwolfach, 1981* (ed. W. Ecklhaus & E. M. DeJager). Lecture Notes in Mathematics, vol. 942, pp. 258–280. Springer.

PARTER, S. V., & RAJAGOPAL, K. R. 1984 Swirling flow between rotating plates. *Arch. Rat. Mech. Anal.* **86**, 305–315.

PEARSON, C. E. 1965 Numerical solutions for time-dependent viscous flow between two rotating coaxial disks. *J. Fluid Mech.* **21**, 623–633.

PESCH, H. J. & RENTROP, P. 1965 Numerical solutions of the flow between two counter-rotating co-axial disks. *J. Fluid Mech.* **21**, 623–633.

RAJAGOPAL, K. R. 1987 Recent developments in the swirling flow of Newtonian and non-Newtonian fluids between rotating plates. *Mechanics Today* (to appear).

ROBERTS, S. M. & SHIPMAN, J. S. 1976 Computation of the flow between a rotating and stationary disk. *J. Fluid Mech.* **68**, 369–388.

SCHULTZ, D. & GREENSPAN, D. 1974 Simplification and improvement of a numerical method for Navier–Stokes problems. In *Proc. Colloquium on Differential Equations, Keszthely, Hungary*, pp. 201–222.

STEWARTSON, K. 1953 On the flow between two rotating co-axial disks. *Proc. Camb. Phil. Soc.* **49**, 333–341.

SZERI, A. Z., SCHNEIDER, S. J., LABBE, F. & KAUFMANN, H. N. 1983 Flow between rotating disks. Part 1. Basic flow. *J. Fluid Mech.* **134**, 103–131.

TRUESDELL, C. & NOLL, W. 1965 The non-linear field theories of mechanics. In *Handbuch der Physik* (ed. S. Flugge), III/3. Springer.

WAGNER, M. H. 1976 Analysis of time dependent non-linear stress growth data for shear and elongational flow of a low-density branched polyethylene line melt. *Rheol. Acta* **15**, 133.

WILSON, L. O. & SCHRYER, N. L. 1978 Flow between a stationary and rotating disk with suction. *J. Fluid Mech.* **85**, 579–596.